J Electroceram (2009) 22:363–368
DOI 10.1007/s10832-007-9399-5

Improved ferroelectricity of strained $SrTiO_3$ thin films on sapphire

R. Wördenweber · E. Hollmann · R. Ott · T. Hürtgen · Tai Keong Lee

Received: 30 March 2006 / Accepted: 15 December 2007 / Published online: 11 January 2008

Abstract Magnetron sputtered and laser deposited $SrTiO_3$ thin films are deposited on CeO_2 buffered sapphire substrates. Their structural properties are investigated and correlated to the dielectric properties of the $SrTiO_3$ films. It is shown, that the biaxial compressive strain imposed by the substrate on the ferroelectric films leads to a considerable increase of the permittivity and tunability of $SrTiO_3$ thin films in technically relevant temperature regimes. Generally, the permittivity and tunability decreases with increasing strain. However, the ferroelectric phase transition of the $SrTiO_3$ films is shifted to higher temperatures compared to that of single crystalline $SrTiO_3$. As a consequence, the permittivity of the films is larger than that of undistorted $SrTiO_3$ single crystals for small strain ($\Delta a/a<0.005$) and temperatures above the Curie temperature. Furthermore, a linear dependence of the loss tangent and the tunability on the permittivity is observed, which indicates, that all three properties are affected by the same mechanism that itself is affected by the lattice strain.

Keywords Ferroelectric films · Oxide film deposition · Impact of strain · $SrTiO_3$ films

1 Introduction

Owing to the strong connection between strain and ferroelectricity, large shifts of the Curie temperature T_c are expected [1, 2] and have been observed [3, 4] in ferroelectric material that is exposed to strain. An ideal method to introduce substantial strain to these materials exists for ferroelectric thin films. Depending on the choice of the substrate, tensile or compressive in-plane strain can be imparted upon epitaxial ferroelectric thin films. It has been speculated [2], that in both cases (tensile and compressive strain) T_c is shifted to higher temperatures resulting in a more profitable temperature dependence of the dielectric constant, ε, that characterizes the permittivity. Due to the strong anisotropy of dielectric response between in-plane and out-of-plane directions, the enhanced Curie–Weiss temperature should be detected only for electric fields (and, thus, polarization) that are oriented parallel to the "elongated direction" (i.e., in-plane oriented electric field for the tensile strain, and out-of-plane oriented electric field for the compressive strain, respectively). This effect has been experimentally demonstrated for planar capacitor configurations on tensile in-plain strained $SrTiO_3$ (STO) on DyScO, whereas capacitors on compressive in-plane strained STO on LSAT did not lead to an improvement of the permittivity [3]. In this paper we show, that in-plane compressive strain induced by CeO_2 buffered sapphire on STO leads to an increase of the permittivity at temperatures above T_c. Furthermore, we will show that the ferroelectric properties strongly depend upon the magnitude of strain.

2 Experimental results and discussion

A series of $SrTiO_3$ (STO) films is grown on CeO_2 buffered r-cut sapphire (Al_2O_3) at various temperatures (650–870 °C) via on-axis magnetron rf sputtering technique (MST) and pulsed laser deposition (PLD). In order to provide identical growth conditions for the STO layer, all CeO_2 buffer layers are

R. Wördenweber (✉) · E. Hollmann · R. Ott · T. Hürtgen · T. K. Lee
Institute for Bio- and Nanosystems (IBN) und cni–Center of Nanoelectronic Systems for Information Technology, Forschungszentrum Jülich,
52425 Juelich, Germany
e-mail: r.woerdenweber@fz-juelich.de

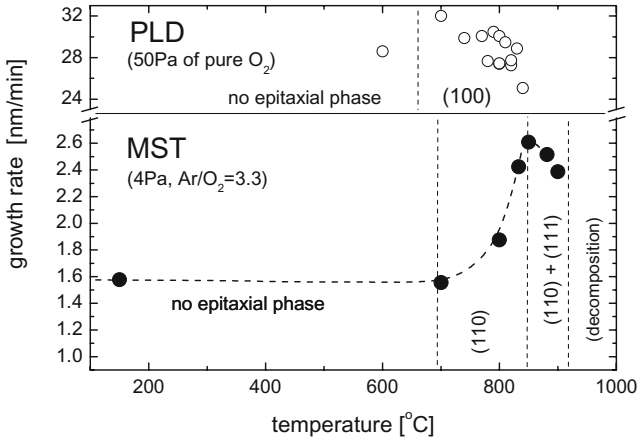

Fig. 1 Growth rate of PLD (*top*) and MST (*bottom*) deposited STO as function of the heater temperature during deposition. The *dashed lines* separate different temperature regimes of different STO phase formations

deposited via MST at identical conditions (i.e., rf-power of 130 W on a 6″ cathode, Ar/O_2 gas mixture of ratio 6.6/1 at a pressure of 13 Pa, and a heater temperature of 850 °C resulting in a deposition rate of 0.5 nm/min) and thickness (40 nm). The STO layers are subsequently deposited via MST and PLD with thicknesses of ~400 nm. The MST depositions are performed in a gas mixture of Ar/O_2 of 3.3/1 at 4 Pa and rf power of 260 W on a 6″ magnetron target. The PLD depositions are performed in pure O_2 atmosphere at a pressure of 50 Pa using a laser power of 10 W at 10 Hz.

The growth rates, phase formation and ferroelectric properties of the STO layers strongly depend upon the preparation method and preparation parameters. The STO growth rates are 1.6–2.6 and 25–32 nm/min for MST and PLD deposition, respectively. Furthermore, depending on the technology and the deposition parameters different structural orientations are obtained. A parameter, that significantly affects the growths and properties of the ferroelectric layer, is given by the substrate temperature, which has been varied in our series in the range of 650–870 °C (heater temperature). A first and very interesting indication for the effect of the substrate temperature upon the STO film growth is given by the deposition rate.

Figure 1 shows the dependence of the STO growth rate on the heater temperature during MST and, for a restricted temperature range, for PLD. It should be noted, that the actual substrate temperature and, especially, the temperature at the substrate's surface strongly differs from the heater temperature. This difference depends strongly on the process and the choice of process parameters. Therefore a direct comparison of the temperatures dependencies obtained for the different deposition technologies should not be considered. Nevertheless, interesting features can be observed. For MST up to about 700 °C heater temperature the growth rate is small, i.e. ~1.6 nm/min. In this temperature regime no epitaxial orientation of the STO on top of the epitaxially grown CeO_2 ((200) orientation) is observed. With the onset of formation of (110)-oriented STO at about 700 °C, the STO growth rate increases significantly by up to ~50%. At about 830 °C another epitaxial phase orientation is starting to grow, i.e., (111)-oriented STO. At this temperature the growth rate for STO starts to decrease again. Finally at temperatures above 900 °C chemical interdiffusion terminates the STO formation.

The STO films obtained via PLD are deposited at a ~10 times larger deposition rate, i.e., 25–30 nm/min. Deposition has only be tested in a restricted temperature regime. Since the samples are glued to the heater, the substrate temperature is probably higher that that for the MST deposition at the same heater temperature. Above ~680 °C the PLD samples show (100) oriented growth of STO, chemical decomposition sets in at about 850 °C.

The structural properties of the films are analyzed by X-ray diffraction (XRD) in Bragg–Brentano geometry. These experiments yield information about the epitaxial orientation of the different layers and their strain. Figure 2(a) shows a typical example of the XRD pattern of a MST sample. The different peaks represent the different epitaxial phases, the area and the angular position of the peaks provide measures for the volume fraction and the strain of the

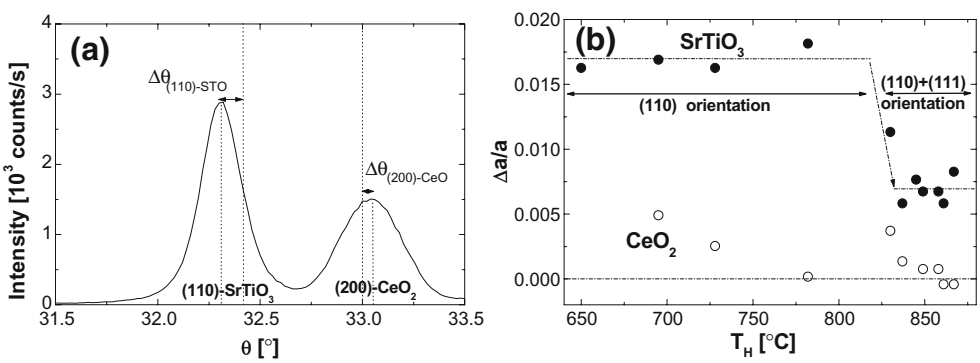

Fig. 2 (**a**) Example of XRD data of a sputtered STO thin film on CeO_2-buffered sapphire and the theoretically predicted angular positions for the (110)-STO and (200)-CeO_2 phases in Bragg–Brentano geometry, (**b**) normalized lattice parameter of the (200)-orientated CeO_2 buffer layer and the (110) and (111) oriented STO layers as function of heater temperature during MST STO-deposition

particular phase, respectively. Adopting a cubical lattice for STO and CeO_2, the lattice constant a of the different layers is given by:

$$a = \gamma \frac{\lambda}{\sin(\theta/2)} \tag{1}$$

with λ representing the X-ray wavelength and γ=1, 1/2, or $1/\sqrt{2}$ for CeO_2(200), STO(100), or STO(110), respectively.

The relative volume fractions of the different epitaxial phases are obtained by angular integration and normalization of the peak of the XRD reflex of the XRD rocking curve:

$$A_{\exp} = \frac{1}{I_{th}} \cdot \int I(\theta) d\omega \, . \tag{2}$$

Here I_{th} represents the theoretical intensity of the examined reflex. The lattice strain can be characterized by the normalized deviation of the lattice parameter from the literature value

$$(\Delta a/a) = \frac{a_{\exp} - a_{th}}{a_{th}} \tag{3}$$

with a_{th} and $a_{\exp}$ representing the theoretical and the measured lattice parameter of the STO phase.

Figure 2(b) shows the distortion of the crystalline lattices of CeO_2 and STO as function of heater temperature during MTS deposition of STO. The strain of the CeO_2 layer is very small ($\Delta a/a$<0.4%) and similar for all samples. This demonstrates that the subsequent deposition of STO at different conditions seems not to affect the structural properties of the buffer layer. With increasing substrate temperature first (110) oriented STO is formed. In contrast to the behavior of CeO_2, the (110) STO phase is strongly distorted. The lattice parameter of the (110) STO phase is about 1.6–1.8% larger than the theoretical value for the STO lattice parameter. At heater temperatures above 830 °C additional to the (110) phase, (111) oriented STO starts to grow. With the inset of the growth of this additional phase, the distortion of the STO lattice is decreased strongly, i.e., to 0.6–0.8% with respect to the undistorted STO lattice. The lattice distortion of the (100) oriented PLD films is generally smaller, i.e. $\Delta a/a \approx 0.4$–0.5%.

The dielectric properties of the films are determined by capacitance measurements of planar capacitors at 1 kHz, 1 MHz, and 2 GHz. Au electrodes (150 nm thickness) are deposited and patterned via lift-off technology upon the ferroelectric thin films (see Fig. 3). In order to improve the resolution of the experiment in most of the cases interdigital capacitor structures are used.

The dielectric properties of the STO film are derived from the experimental data using the model of parallel capacitors [5]. In this model the total capacitance is given by the sum of the different contribution in parallel configuration:

$$C_{\text{total}} = C_{\text{STO}} + C_{\text{air}} + C_{\text{substrate}} + C_{\text{rest}} \tag{4}$$

that arise from the capacitance of the STO layer, the area above the capacitor (air with $\varepsilon_{\text{air}} \approx 1$), the substrate, and the stray capacitance of the experiment (e.g., contributions from cables ect), respectively. The latter can be neglected due to the calibration of the experimental setup. For small enough capacitor gaps or thick enough STO films, the different contributions of our planar capacitor device are given by [5–7]:

$$C_i = \varepsilon_0 \varepsilon_i d \cdot f_i(s, l, h_i) \tag{5}$$

with the different contributions $f_{\text{STO}} = 0.25\pi/[\ln 2 + (\pi \cdot s/(4 \cdot h_{\text{film}}))]$, $f_{\text{air}} = 2\pi^{-1} \ln(4l/s)$ and $f_{\text{substrate}} = \pi^{-1} \ln(16 h_{\text{substrate}}/\pi s)$ Here s and d represent the width and length of the capacitor gap, h_i the thickness of the layer, and l the length of the electrodes. With Eqs. (4) and (5), the geometric parameters of the planar devices and the permittivities of air ($\varepsilon_{\text{air}} \approx 1$) and substrate ($\varepsilon_{\text{sapphire}} \approx 10$–11), we can evaluate the permittivity of the STO layer from the experimental data of the capacitance measurement.

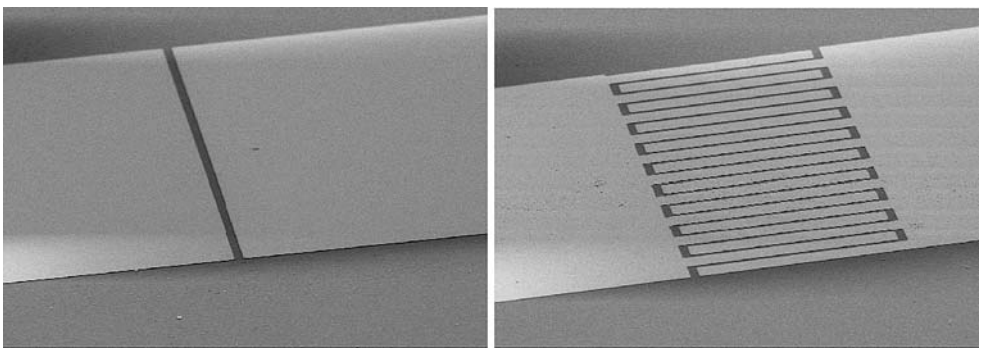

Fig. 3 SEM images of different types of planar capacitors on the STO thin films. The electrides are 500 μm wide, the size of the gap ranges between 2 and 10 μm

The losses $tan\delta_{STO}$ and the tunability n_{STO} of the STO layers are obtained from the experimental data using the expressions:

$$\tan\delta_{STO} = \frac{C_{total}\cdot\tan\delta_{total} - C_{air}\cdot\tan\delta_{air} - C_{substrate}\cdot\tan\delta_{substrate}}{C_{total} - C_{air} - C_{substrate}} \quad (6)$$

$$\cong \frac{C_{total}\cdot\tan\delta_{total}}{C_{total} - C_{air} - C_{substrate}}$$

and

$$n_{STO} = \frac{\varepsilon_{STO}(E_{DC}=0)}{\varepsilon_{STO}(E_{DC})} - 1 \quad (7)$$

where $tan\delta_i$ represents the loss tangent of the different components and E_{DC} is the electric DC field that is used for the tuning of the permittivity.

Figure 4 shows the temperature dependence of the permittivity of the PLD deposited STO layers (thickness of 500 nm) and, for comparison, the permittivity of a STO single crystal. In pure, unstressed form, STO is an incipient ferroelectric. It remains paraelectric down to 0 K. This is among others visible in the perfect Curie–Weiss behavior ($\varepsilon \propto 1/(T-T_c)$) with a Curie temperatures $T_c \approx 0$ shown in Fig. 4 for the measurement on the STO single crystal. In contrast to the single crystal, the films show a Curie–Weiss like behavior with $T_c >> 0$ only at high temperatures $T > 150$ K. Moreover, the temperature dependence of the permittivity of the films shows a pronounce maximum at low temperature. The position of the maximum depends upon the preparation parameter, it is observed for temperatures around 60–120 K. This maximum is associated with a Curie temperature, that is clearly enhanced in the STO films [6, 7]. Finally, it should be noticed, that at high temperatures the permittivity of the films is larger than the permittivity of the single crystal.

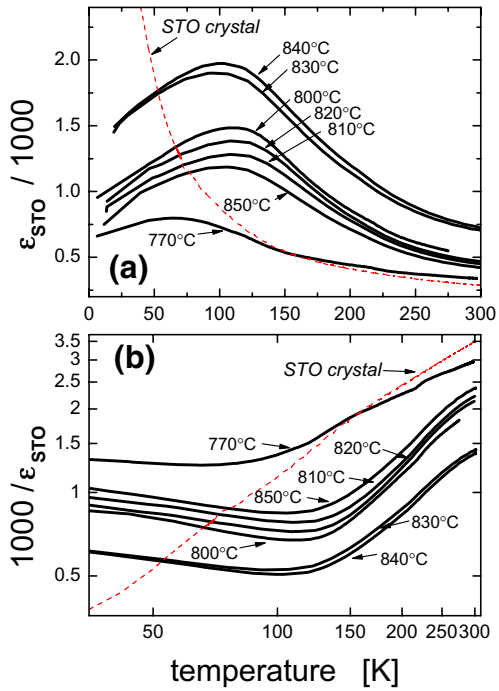

Fig. 4 Temperature dependence of the permittivity (**a**) and inverse permittivity of STO films deposited via PLD at different heater temperatures (**b**). Additionally the data of single crystalline STO is given, which is obtained from measurements of a planar capacitor on a single crystalline STO substrate

In order to discuss and compare the different data, let us consider the structural dependence of the ferroelectric properties. Figure 5 shows the permittivity, losses, and tunability of the films as function of the normal lattice distortion at 77 K. All three properties decrease in a similar way with increasing lattice distortion. The distortion represents an expansion of the lattice constant $a_\perp$ normal to the film surface. Since the volume of the unit cell should be conserved, the in-plane STO lattice constant $a_\parallel$ will be compressed by 0.2–1.6%. This is consistent with the structural restrains from the nearly undistorted CeO_2 buffer layer (see Fig. 2) that defines the starting condition for the epitaxial STO phase. The epitaxial STO layers grow under ~45° orientational in-plane rotation on top of the CeO_2, i.e., the [100] and [111] directions of STO and CeO_2, respectively, are oriented parallel. Thus, a biaxial compressive strain characterized by a reduction of the lattice parameter of $\Delta a_\parallel / a = 0.02$ is expected for the first monolayers of STO. This strain will then relax over the thickness of the STO layer.

It is known, that strain is one of the important factors affecting the ferroelectric properties since it is directly related to the ionic polarization in ferroelectrics [8–11]. It has been demonstrated, that strain modifies the ferroelectric phase transition, the permittivity, and the dielectric tuning [4, 12–22]. Generally it can be assumed, that with increasing stain (tensional as well as compressive) the permittivity and ferroelectric tuning will decrease. However, it is also speculated and has been confirmed experimentally, that strain can lead to a modification of the Curie temperature. Due to the strong anisotropy of dielectric response between in-plane and out-of-plane electric field directions, an enhanced Curie–Weiss temperature is expected only for measurements of the polarization with the electric field oriented parallel to the elongated crystallographic lattice constant. This is the in-plane direction for tensile strain, and the out-of-plane direction for compressive strain, respectively. Based on the theoretical equations derived from Landau theory using the electrostrictive constants [15], the “in-plane” and “out-of-plane” permittivities of compressive (100)-STO will be theoretically lower and higher than that of the unstrained STO, respectively. Therefore, the expected modification of T_c should depend upon the orientation of the film and the orientation of the electric field, which is defined by the arrangement of the electrodes.

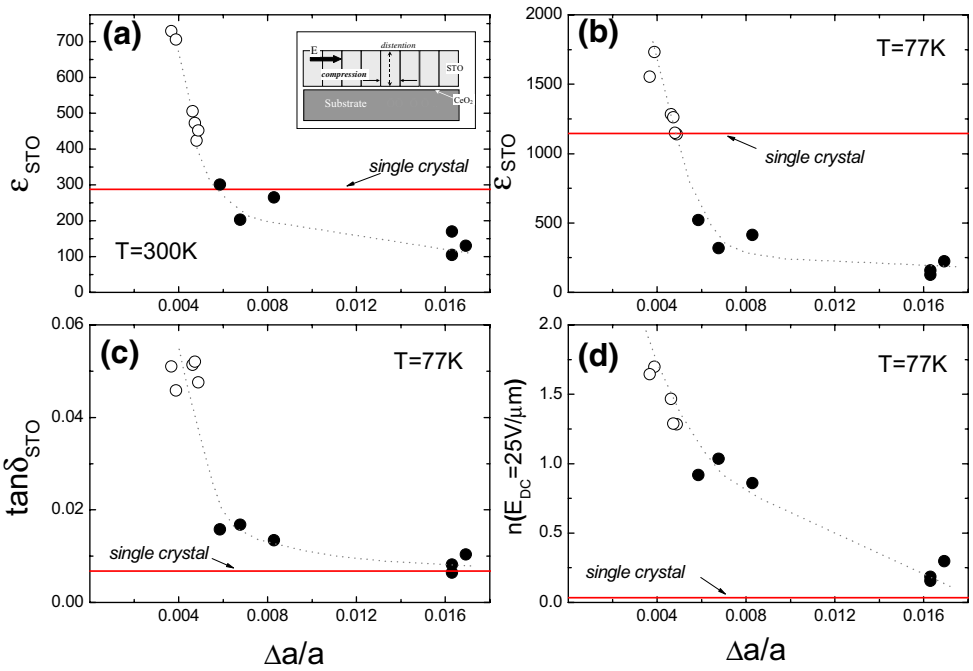

Fig. 5 Permittivity ((**a**) and (**b**)), loss tangent (**c**), and tunability (**d**) at 77 K (and 300 K in (**a**)) as function of the normalized lattice distortion normal to the substrate surface for PLD (*open circles*) and MST (*solid circles*) STO films measured at 1 MHz

The increase of T_c can cause an increase of the permittivity and, as a consequence, increase of the dielectric tuning at elevated temperature. This has been demonstrated for thin films of STO on $DyScO_3$ with tensile in-plane strained STO [4, 18]. However, due to experimental results of STO films on LSAT it has been speculated, that for compressive strained STO the Curie temperature is increased, but the permittivity is decreased.

On the one hand, we do observe the general tendency, that the permittivity and the tuning decreases with increasing strain for the STO films on CeO_2 buffered sapphire (see Fig. 5). On the other hand, for all samples the ferroelectric phase transition is shifted to higher temperatures compared to $T_c \approx 0$ of the single crystalline STO [6, 7]. As a consequence, the permittivity of the films is larger than that of the undistorted STO single crystal for small strain ($\Delta a/a < 0.005$) and temperatures above the Curie temperature. It seems, that also biaxial compressive strain can lead to a considerable increase of the permittivity and tuning.

Finally, we consider the mutual dependence of the different properties of the ferroelectric layers. Figure 6 indicates, that the permittivity, the loss tangent, and the tunability seem to be correlated. We observe a linear dependence of the loss tangent and the tunability on the permittivity. The Kramers–Kronig integral relation is often used to describe the relation between the real and imaginary part of the dielectric susceptibility. The linear correlation between the different parameters might be taken as an indication, that all three parameters are affected by the same mechanism that itself is affected by the lattice strain.

3 Conclusions

Magnetron sputtered and laser deposited $SrTiO_3$ thin films were fabricated on CeO_2 buffered sapphire substrates. The structural properties and, especially, the strain are investigated and correlated to the dielectric properties of the films.

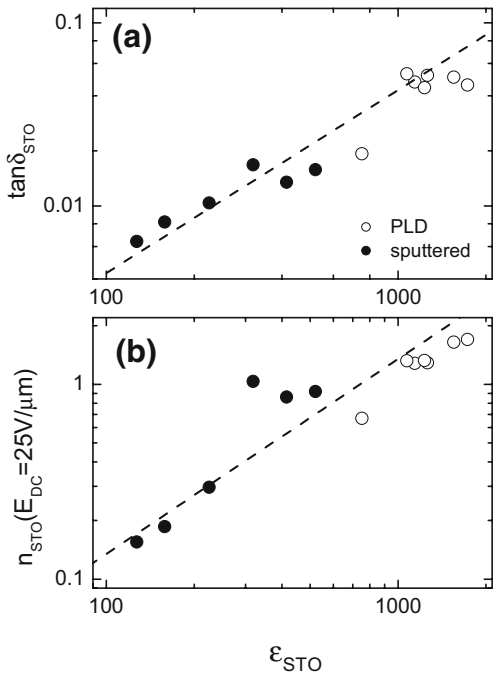

Fig. 6 Double logarithmic plot of the dielectric loss $\tan\delta_{STO}$ (**a**) and tunability $n_{STO}(U_{dc}=100\ V)$ (**b**) of the PLD (*open symbols*) and MST (*solid symbols*) STO films at 77 K as function of the permittivity ε_{STO} measured at 1 MHz. The *dashed lines* indicate the linear dependence between the different properties

Generally, the permittivity and the tuning decreases with increasing strain for the STO films on CeO_2 buffered sapphire. However, the ferroelectric phase transition of the STO films is shifted to higher temperatures compared to that of single crystalline STO ($T_c \approx 0$). As a consequence, the permittivity of the films is larger than that of that of the undistorted STO single crystal for small strain ($\Delta a/a < 0.005$) and temperatures above the Curie temperature. Furthermore, we observe a linear dependence of the loss tangent and the tunability of the permittivity. This correlation between the different parameters might be taken as an indication, that all three parameters are affected by the same mechanism that itself is affected by the lattice strain.

It seems, that not only biaxial tensile strain, but also biaxial compressive strain can lead to a considerable increase of the permittivity and tuning of $SrTiO_3$ thin films in technically relevant temperature regimes. Considering the advantage of the use of sapphire as a low-loss technical substrate, this makes this system—$SrTiO_3$ on CeO_2 buffered sapphire—an interesting system for rf tuning devices or phase shifters.

Acknowledgement The authors would like to thank G. Pickartz, S. Bunte, R. Kutzner, H.P. Bochem, M. Nonn, N. Klein, and A. Offenhäuser for their valuable support.

References

1. A.F. Devonshire, Phil. Mag. Suppl. **3**, 85–130 (1954)
2. N.A. Pertsev, A.G. Zembilgotov, A.K. Tagantsev, Phys. Rev. Lett. **80**, 1988–1991 (1998)
3. S.K. Streiffer, J.A. Eastman, D.D. Fong, C. Thompson, A. Munkholm, M.V. Ramana Murty, O. Auciello, G.R. Bai, G.B. Stephenson, Phys. Rev. Lett. **89**, 67601 (2002)
4. J.H. Haeni, P. Irvin, W. Chang, R. Uecker, P. Reiche, Y.L. Li, S. Choudhury, W. Tian, M.E. Hawley, B. Craigo, A.K. Tagantsev, X.Q. Pan, S.K. Streiffer, L.Q. Chen, S.W. Kirchoefer, J. Levy, D.G. Schlom, Nature **430**, 758 (2004)
5. O.G. Vendik, M.A. Nikol, skii, Tech. Phys. **46**(1), 112–116 (2001)
6. R. Ott, P. Lahl, R. Wördenweber, Appl. Phys. Lett. **84**, 4147 (2004)
7. T. Hürtgen, Thesis, Univ. Aachen (2004)
8. W.J. Merz, Phys. Rev. **78**, 52 (1950)
9. J.C. Slater, Phys. Rev. **78**, 748 (1950)
10. P.W. Forsbergh Jr., Phys. Rev. **93**, 686 (1954)
11. G.A. Samara, A.A. Giardini, Phys. Rev. **140**, A954 (1965)
12. T. Schimizu, Solid State Commun. **102**, 523 (1997)
13. W. Chang, J.S. Horwitz, J.M. Pond, S.W. Kirchoefe, D.B. Chrisey, Mater. Res. Soc. Symp. Proc. **526**, 205 (1998)
14. W. Chang, J.S. Horwitz, W.J. Kim, J.M. Pond, S.W. Kirchoefer, C.M. Gilmore, S.B. Qadri, D.B. Chrisey, Integr. Ferroelectr. **24**, 257 (1999)
15. N.A. Pertsev, A.K. Tagantsev, N. Setter, Phys. Rev. B **61**, R825 (2000)
16. N.A. Pertsev, A.K. Tagantsev, N. Setter, Phys. Rev. B **65**, 219901 (E) (2002)
17. W. Chang, S.W. Kirchoefer, J.M. Pond, J.S. Horwitz, L. Sengupta, J. Appl. Phys. **92**, 1528 (2002)
18. W. Chang, S.W. Kirchoefer, J.M. Pond, J.A. Bellotti, S.B. Qadri, J.H. Haeni, D.G. Schlom, J. Appl. Phys. **96**, 6629 (2004)
19. R. Wördenweber, R. Ott, P. Lahl, J. Electroceramics **13**, 223–227 (2004)
20. C.L. Canedy, H. Li, S.P. Alpay, L. Salamanca-Riba, A.L. Roytburd, R. Ramesh, Appl. Phys. Lett. **77**, 1695 (2000)
21. T. Yamada, K.F. Astafiev, V.O. Sherman, A.K. Tagantsev, P. Muralt, N. Setter, Appl. Phys. Lett. **86**, 142904 (2005)
22. T. Yamada, J. Petzelt, A.K. Tagantsev, S. Denisov, D. Noujni, P.K. Petrov, A. Mackova, K. Fujito, T. Kiguchi, K. Shinozaki, N. Mizutani, V.O. Sherman, P. Muralt, N. Setter. Phys. Rev. Lett. **96**, 157602 (2006)